

Polysulfone (Psf) Mixed Matrix Membrane incorporating Titanium Dioxide (TiO₂)/Polyethylene Glycol (PEG) for the removal of copper

Vasuumathi A/P Ilango Mathialagan ^a, Sivaneswari A/P M Devarajoo ^a, Hafiza Shukor ^{b*}, M. N. Aiman Uda ^c, Noor Fazliani Shoparwe ^d, Muaz Mohd Zaini Makhtar ^e, and Nor' Izzah Zainuddin ^f

^aFaculty of Chemical Engineering Technology, University Malaysia Perlis, 02600 Arau, Perlis, Malaysia

^bCentre of Excellence for Biomass Utilization, Faculty of Chemical Engineering Technology, University Malaysia Perlis, 02600 Arau, Perlis, Malaysia

^cInstitute of Nano Electronic Engineering, Universiti Malaysia Perlis (UniMAP), 01000 Kangar, Perlis, Malaysia

^dGold, Rare Earth & Material Technopreneurship Centre (GREAT), Faculty of Bioengineering and Technology, University Malaysia Kelantan, Jeli Campus, 17600 Jeli, Kelantan, Malaysia

^eBioprocess Technology Division, School of Industrial Technology, Universiti Sains Malaysia, Gelugor 11800, Pulau Pinang, Malaysia

^fIndah Water Konsortium, Lorong Perda Utama 13, Bukit Mertajam 14300, Pulau Pinang

* Corresponding author. Tel.: +6-019-286-4649; e-mail: hafizashukor@unimap.edu.my

Received 18 January 2024, Revised 31 March 2024, Accepted 7 May 2024

ABSTRACT

The global increasing contamination of water resources with toxic metals such as copper (Cu), poses severe threats to human health and aqueous ecosystems. Therefore, the ultrafiltration mixed matrix membranes (UF MMMs) possess an applicable approach for the removal of copper ions. This novel fabricated technology can be applied in various wastewater treatment systems for the removal of heavy metals, especially copper. MMMs were fabricated by blending polysulfone (Psf) with additives into the dope solution via the phase inversion method by incorporating titanium dioxide (TiO₂) and polyethylene glycol (PEG) in Psf MMMs. Seven Psf MMMs samples labelled M0 to M6, each with its own formulation, were prepared and tested for density, porosity, and degree of Cu retention. MMMs were further characterized via Fourier transform infrared spectroscopy (FTIR), which revealed the range of the IR spectrum of Psf polymer membrane from 1319 cm⁻¹ to 1600 cm⁻¹, 1650 cm⁻¹ to 3400 cm⁻¹ for PEG, and 800 cm⁻¹ to 3600 cm⁻¹ for TiO₂ NPs. As for the scanning electron microscopy (SEM), M6 (Psf/TiO₂/PEG 6000) was found to be the most dense and highest porous morphology asymmetric Psf MMM. The retained percentage of Cu and flux for M6 attained the highest value of 80.3% and 136.99 L/m².h respectively, whereas for the neat Psf membrane, M0 exhibited the lowest retained percentage of Cu and flux, about 25.8% and 61.64 L/m².h. The inclusion of pore former and additives has shown an improvement of 54.5% in the copper rejection. Moreover, M6 displayed the highest antifouling properties compared to other Psf MMMs. This study proves that PEG and TiO₂ additives have significant potential to improve membrane performance due to the highest percentage of Cu retained on the surface of the membrane as adsorptive separation on Psf MMMs.

Keywords: Copper, Mixed matrix membrane, Polysulfone, Ultrafiltration

1. INTRODUCTION

Water pollution is becoming a global concern due to massive population growth, rapid industrial development, and gradually accelerating urbanization. Human activities such as mining, mineral processing, and metallurgical operations are contributing to wastewater pollution [1]. Heavy metals are among the most dangerous pollutants released. Heavy metals (HMs) are any metallic elements with a relative high density compared to water, or, in other words, heavy metals are metals that have a density greater than 5 g/cm³ [2]. The effects of HM pollution include damage to marine life, serious health issues for humans due to unhygienic water supply, and damage to the environment. The removal of HM via membrane technology meets the sixth goal of the Sustainable Development Goals (SDG), which is to ensure clean water and sanitation by the 2030 timeline.

Hence, membrane technologies offer a one-of-a-kind opportunity for the removal of heavy metals via pressure-driven membrane separation [3]. One of the innovative membrane technologies is introduced in this, which is "Development of a Novel PSF Mixed Matrix Membrane," also known as a "Green Technology," that can be used for HM removal, especially copper in the present study. MMMs, known as organic and inorganic nanocomposite, consist of nanoparticle-based membranes, also known as nano-incorporation membranes. In contrast to ordinary membranes, MMMs are composed of an organic polymer embedded with inorganic fillers such as titanium dioxide (TiO₂), polyethylene glycol (PEG), zeolites, multi-walled carbon tubes (MWCT), and so forth. Nanoparticles (NPs) can be used to make polymer and NP-blend membranes for a couple of different reasons.

One goal is to create membranes with a desired structure because of interactions between the nanoparticle surface, polymer chains, and solvents during membrane formation. The membrane's hydrophilicity and pore size were enhanced as a result of these membrane modifications. The presence of nanoparticle functional groups and their hydrophilic characteristics is also being used to control membrane fouling. Moreover, a variety of polymers, such as polyvinylidene fluoride (PVDF), polyamide (PA), polysulfone (Psf), and polyethersulfone (PES), can be used as membranes. The blended mixed matrix membranes, which comprise polymers, solvents, and additives, are believed to achieve greater performance compared to the pristine polymeric membranes. Membrane performance can be improved during the fabrication process, not only for resistance to extremes in process conditions, but also for improved mixture resolution during Cu separation.

The research questions include how to fabricate and characterize the chemical and physical properties of Polysulfone Mixed Matrix Membrane (Psf MMM) for copper (Cu) removal, how to evaluate the performance of the fabricated Psf MMM for copper removal, and what is the fouling mechanism and the factors that lead to this phenomenon on fabricated Psf MMM for copper removal.

2. MATERIALS AND METHODS

2.1. Materials

The material used in this research was copper (II) sulfate – 5- hydrate C0961-21412702 (purity 100%) that was purchased from Sigma Aldrich (USA) and is one of the main chemical reagents utilised during permeation test as well as to obtain the calibration curve. Psf (35000 MWCO), dimethylacetamide (DMAc), polyethylene glycol (PEG) and titanium dioxide (TiO₂) were the membrane materials used to make the dope solution and subsequently it was fabricated to obtain a flat sheet mixed matrix membrane. These membrane materials were also obtained from Sigma Aldrich (USA). Nitrogen gas was used to provide pressure during the dead-end filtration test. Distilled water that was obtained from the UniMAP laboratory acted as the coagulation bath during the phase inversion method.

2.2. Methods

Non-solvent induced phase inversion method (NIPS) was applied to fabricate Psf MMMs. Before the fabrication process, the dope solution was made according to the fixed formulations as depicted in Table 1. As an initial step, Psf

polymer was dried for 20 hours at 80°C in the oven before being utilised. In the oven, materials that are combustible or can produce flammable vapours were not used. After that, all the Psf for the 8 respective samples were weighed and segregated into separate containers. In order to make a proper dope solution, additives should be mixed first in the solvent followed by the polymer. All the additives and the solvent were weighed accordingly following the formulations.

Then, the dope solution was prepared by mixing the additive, which was the TiO₂, in the solvent N-N-dimethylacetamide (DMAc) at room temperature using a magnetic stirrer. Hot plates were utilized to enhance the efficiency of nanoparticle dispersion in the solvent. After that, PEG was added and dissolved into the solution and stirred continuously. A thermometer was utilized to measure the mixing process at 90°C. The casting solution needs to be mixed well under continuous agitation on the hot plate at 90°C for 5 hours [4]. When making the dope solution, an important rule of thumb was to avoid the solution coming into contact with distilled water.

During the fabrication process, the casting knife was utilised to spread the dope solution over a glass plate at 200 µm [5]. The forward speed used to cast the porous, thin film membrane was 20 rev/s. The thin film membrane then underwent a 30-second dry-wet phase inversion once the casting process was completed. After that, the asymmetric flat sheet Psf MMMs plate will be immersed into the non-solvent medium of distilled water for solvent and non-solvent exchange. The resulting film membrane was then dried at room temperature before it was cut into the desired shapes. Finally, the membrane was dried for 24 hours at room temperature.

The feed solution, copper sulphate pentahydrate solution was utilised to test the ultrafiltration membrane's performance in terms of copper rejection rate and flux. To obtain copper sulphate pentahydrate solution, 0.5 g of copper ions were dispersed in 1 L of deionized water. The solution was then centrifugated for an hour to obtain a homogenous solution. The pH of copper sulphate pentahydrate solution was adjusted to 7.70 by pH meter with the aid of 1 M of HCl and 1 M of NaOH [6]. In addition, the concentration of copper solution was fixed at 500mg/L by using a UV spectrophotometer at a wavelength of 680–860 nm. Five different concentrations of Cu were prepared from 100 mg/ml, 200 mg/ml, 300 mg/mL, 400 mg/mL and 500 mg/mL to obtain the calibration curve of Cu.

Table 1. The dope solution formulations

Membrane	UF membrane	Psf (wt. %)	DMAc (wt. %)	Mixed matrix membrane (MMM)	
				TiO ₂ (wt. %)	PEG (wt. %)
M0	Psf Membrane	21	79.0	-	-
M1	Psf + TiO ₂ Membrane	21	78.5	0.5	-
M2	Psf + TiO ₂ + PEG 600 Membrane	21	77.0	0.5	1.5
M3	Psf + TiO ₂ + PEG 1000 Membrane	21	77.0	0.5	1.5
M4	Psf + TiO ₂ + PEG 1500 Membrane	21	77.0	0.5	1.5
M5	Psf + TiO ₂ + PEG 4000 Membrane	21	77.0	0.5	1.5
M6	Psf + TiO ₂ + PEG 6000 Membrane	21	77.0	0.5	1.5

2.3. Characterization

The characterization process specifies the structural morphology and functionality of the membrane due to the addition of new components such as pore formers and nanoparticles into the membrane matrix [7]. Therefore, the characterization process is a crucial step that is done after the surface modification process to confirm if the changes made to the membrane structure are applicable and allow smooth performance of the membrane [7]. Membrane characterization can be segregated into physical and chemical characteristics.

2.3.1. Physical Characteristics

Physical characteristics of the membrane comprise Scanning Electron Microscopy (SEM), Contact Angle (CA) Evaluation, and membrane porosity which mainly focuses on the morphology and pore size of the membrane.

2.3.1.1. Scanning Electron Microscopy (SEM)

SEM was used to characterise membrane surface and volume structures. It is considered a primary approach that provides information on the morphology and topography of prepared membranes. The data is obtained by scanning the membrane surfaces with a focused electron beam [7]. Furthermore, SEM was also used to analyse the pore size in porous membranes [8] whereas for dense membranes the thickness of the selective layer was analysed. Before scanning in the SEM, the sample was made sure it was in a solid phase. In this SEM analysis, a plain view and cross-sectional view of the membrane were observed.

The steps for SEM testing first began by cutting the active part of the membrane into samples with dimensions of 1 cm × 1 cm, respectively, for both cross-section view and plain view. Next, for the cross-sectional view, the sample was prepared by dispersing it into liquid nitrogen for 1 minute to eliminate surface bends and for better images and then was fractured. This method, commonly known as the freeze-drying method, allows for better imaging of the membrane's interior cross-section. The procedure starts by collecting liquid nitrogen and storing it in a thermos flask to avoid vaporization, as liquid nitrogen is easily volatile when exposed to air or the environment. The cut samples were then stuck onto cardboard. Safety gloves and a face shield were worn before handling the liquid nitrogen as a safety measure. The liquid nitrogen was then poured into a beaker until the membrane was fully dipped. The dipped membrane will be then removed from the beaker with the aid of forceps, and the membrane will be cracked. The crack sound should be heard, as it is very essential while cracking the membrane. The cracked section was then sent for SEM analysis. During SEM analysis, a double-sided carbon adhesion foil was used as a holder to mount the sample vertically [9]. The sample was then coated with a thin layer of platinum under vacuum using sputter coating to neglect electrostatic charging. The coating layer thickness ranged from 2 nm to 5 nm and the metal utilised was taken into consideration as it can have an impact on the coating structure [10]. SEM test was then carried out. The SEM

machine used for testing was the Xhr Extreme High-Resolution Field Emission Scanning Electron Microscope (Xhr-Fesem) Model Fei Verios 460L. The samples were then sent to the Science and Engineering Research Centre, Universiti Sains Malaysia (SERC USM) for testing.

2.3.2. Chemical Characteristics

Chemical characteristics comprise Fourier transform infrared spectroscopy (FTIR), which mainly focuses on functional groups available in the fabricated membrane.

2.3.2.1. Fourier Transform Infrared Spectroscopy (FTIR)

FTIR was used to characterize the membrane surface and determine the functional groups such as hydroxyl (OH-) and carbonyl (C=O) [11] that are able to capture spectrum data in a wide spectral range of 4000–425 cm⁻¹. FTIR analysis can be performed on all phases (solid, liquid, or gas). The sample preparation was initiated by cutting the membrane into dimensions of 1 cm × 1 cm. For FTIR spectroscopy, attenuated total reflectance (ATR) is one of the most commonly utilized sampling technologies. ATR is a sampling technique that uses light to extract structural and compositional information from a sample. The FTIR will be fitted with an OMNI-sample attenuated total reflection (ATR) smart accessory and connected to a diamond crystal with an incidence angle of 45°. An average of 32 scans was taken to record each spectrum with a resolution of 4 cm⁻¹. The FTIR machine that was used to test the samples is the Perkin Elmer Spectrum 65, USA.

2.3.2.2. Membrane Porosity

The dry weight of the membrane was used to assess its porosity. The membrane was immersed in deionized water [12]. Once the surplus wet membrane has been removed with filter paper, the weight of the wet membrane was measured. The wet membrane was then dried for 10 hours in a 25°C oven. The dry membrane's measured weight was calculated using Equation (1) [4]:

$$\varepsilon(\%) = \frac{W_w - W_d}{W_w - \frac{W_d}{d_w} + \frac{W_d}{d_p}} \times 100\% \quad (1)$$

where ε is the membrane porosity, W_w is the wet membrane weight (g), W_d is the dry membrane weight (g), D_w is the pure water density (1.0 g/cm³) and D_p is the polymer density (1.37 g/cm³).

2.3.2.3. Membrane Porosity

Pure water flux (PWF) and porosity data was used to calculate average pore radius size (rm). Porosity data obtained from Guereout-Elford-Ferry equation [13]. Equation (2) was applied to calculate the average pore radius size (rm):

$$rm = \frac{\sqrt{(2.9 - 1.75 \text{ Porosity}) 8\eta l Q}}{\text{Porosity} \times A \times \Delta P} \quad (2)$$

where η is the water viscosity (8.9×10^{-4} pa·s), l is the membrane thickness (m), q is the pure water flux (m^3/s), a is the area (m^2), and ΔP is the operating pressure (1 bar).

2.3.2.4. Contact Angle (CA) Evaluation

At typical room temperature, the hydrophilicity of the membrane surface was determined using a contact angle goniometer [7]. The contact angle was measured immediately once the deionized water was dropped on the membrane's surface. A water droplet of 5 μL size was mounted on the dry membrane layer at room temperature with the aid of motor-driven micro syringe. An imaging software named Angle Meter PRO Plus was then used to capture images of the water droplet on the surface of the membrane in order to evaluate the contact angle [8]. To avoid experimental error, an average of 10 readings were obtained for each sample, and the mean values were then determined.

2.4. Membrane Permeation Test for Copper Removal

The performance of the Psf membrane was examined on the basis of pure water flux (PWF), copper flux, and rejection. The dead-end cell will be supplied with compressed nitrogen air. Nitrogen gas pressure will filter out the copper molecules and cause permeate flow. The membrane was tested at room temperature with a pressure of 3 bar. The pure water flux of the membrane was also measured. Quantitative analysis was used to calculate PWF, the equation shown in Equation (3) [9]:

$$J_{WF} = \frac{V}{A_m t} \quad (3)$$

where J_{WF} is the pure water flux ($\text{L}/\text{m}^2 \cdot \text{h}$), V is the permeate volume (L), A_m is the effective filtration area (m^2), and t is the measurement time (h).

Cu solution was brought at a pressure of 3 bar for one hour after pure water filtration. The concentration of Cu before filtration and permeate after the experiment was measured using UV-VIS Spectrophotometer.

At different interval of time, the Cu flux was calculated by using Equation (4) [10]:

$$F_{Cu} = \frac{V}{A_m t} \quad (4)$$

where F_{Cu} is the Cu flux ($\text{L}/\text{m}^2 \cdot \text{h}$), V is the permeate volume (L), A_m is the effective filtration area (m^2), and t is the measurement time (h).

Apart from that, the removal of Cu as retentate was calculated using Equation (5):

$$R_{Cu} = \frac{[Cu]_{in} - [Cu]_{out}}{[Cu]_{in}} \quad (5)$$

where R_{Cu} is the retentate of Cu ($\text{L}/\text{m}^2 \cdot \text{h}$), $[Cu]_{in}$ (mol/L) is the initial concentration of Cu in the feed solution, and $[Cu]_{out}$ (mol/L) is the final concentration of Cu.

2.5. Membrane Fouling Resistance Evaluation

Relative flux reduction (RFR) was used to calculate fouling resistance, as shown in the Equation (6):

$$RFR(\%) = 1 - \frac{J_{Cu}}{J_{WF}} \quad (6)$$

where RFR is the relative flux reduction while J_{Cu} is tested solution (Cu solution) permeate flux ($\text{L}/\text{m}^2 \cdot \text{h}$), and J_{WF} is the initial water flux.

Moving on, the membrane was cleansed for 15 minutes with distilled water, and filtration will resume with the addition of pure water to the feed tank. The PWF measurement was used for the second time in order to assess the membrane's flow recovery [11]. The flux recovery of the membrane is calculated using Equation (7):

$$FRR(\%) = \frac{J_{WF2}}{J_{WF}} \times 100\% \quad (7)$$

where J_{WF2} will be the PWF after washing step ($\text{L}/\text{m}^2 \cdot \text{h}$).

3. RESULTS AND DISCUSSION

3.1. Fourier Transform Infrared Spectroscopy (FTIR)

Fourier transform infrared spectroscopy (FTIR) was used to perform the chemical characterization for the fabricated Psf MMMs. Generally, FTIR is the most effective alternative analysis to elucidate the functional group of the membrane. The conducted analysis was performed at wavelengths ranging from 4000 cm^{-1} to 650 cm^{-1} . Figure 1 depicts the FTIR spectra of pure Psf (M0), Psf/TiO₂ (M1), Psf/PEG 600/TiO₂ (M2), Psf/PEG 1000/TiO₂ (M3), Psf/PEG 1500/TiO₂ (M4), Psf/PEG 4000/TiO₂ (M5), and Psf/PEG 6000/TiO₂ (M6), respectively.

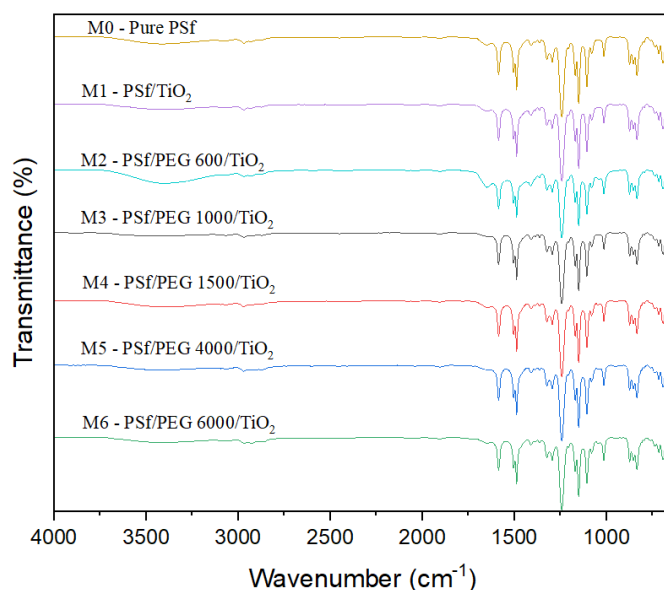


Figure 1. FTIR spectra of Psf MMM, M0-M6

The bands at 1583 cm^{-1} and 1502 cm^{-1} are attributed to the significant reflection of benzene ring stretching for the pure Psf membrane, M0. It can be seen that the sulfone C - SO₂ - C is demonstrated to stretch both symmetrically and asymmetrically. The symmetrical stretching can be observed at 1149 cm^{-1} while the asymmetrical stretching is at 1319 cm^{-1} and 1272 cm^{-1} [14]. Moreover, a strong reflectance of benzene ring stretching can be seen at 1583 cm^{-1} up to 1502 cm^{-1} [15]. According to [16], the individual bands at 861 cm^{-1} and 698 cm^{-1} exhibit aromatic C-H bending. Apart from that, the absorption of the Psf layer can be assessed through O=S=O values of 1000 cm^{-1} - 1300 cm^{-1} and C=C values of 1400 cm^{-1} - 1600 cm^{-1} respectively. The Psf support displays two additional minor bands at 1386 cm^{-1} and 1366 cm^{-1} . These additional minor bands reveal the distinct presence of methyl groups in Psf.

Next, the Psf/TiO₂ membrane, M1 showcased the bending vibration of (Ti-O-Ti) bonds in the TiO₂ lattice, which can be observed in the compact band from 500 cm^{-1} to 600 cm^{-1} . Moving on, the intermolecular interaction of the hydroxyl group (OH) on the Psf polymer chain along with TiO₂ surface was present with the evidence of the narrow band from 3600 cm^{-1} to 3400 cm^{-1} . All of the functional groups match those present in the Psf repeating units. C-O spanning at 1101 cm^{-1} as well as the peak at 600 cm^{-1} to 1000 cm^{-1} proved the presence of oxygen-containing groups of TiO₂ and the successful stretching Ti-O-Ti. The good accordance demonstrates the validity of the synthesized Psf membrane and the elimination of any impurities or solvents that can potentially affect the membrane separation performance.

Other than that, Psf/PEG/TiO₂ membranes from M2 - M6 revealed aliphatic C-H stretching changes to a higher wavelength range of 861 cm^{-1} and 698 cm^{-1} for pristine Psf to 866 cm^{-1} and 704 cm^{-1} for Psf/PEG. It was also observed that the intensity of the stretching decreased when compared with pure Psf. The band location of benzene ring stretching varies from 1583 cm^{-1} to 1502 cm^{-1} for pure Psf whereas for Psf/PEG mix membrane, the band location varies from 1585 cm^{-1} and 1503 cm^{-1} . Furthermore, the band positions of symmetric and asymmetric sulfones shifted to higher wavenumbers from 1149 cm^{-1} , 1319 cm^{-1} , and 1292 cm^{-1} to 1150 cm^{-1} , 1320 cm^{-1} , and 1294 cm^{-1} . Thus, this change confirms the existence of an interaction between PEG and Psf [17]. There might be situations where the positively charged double C=C groups of PEG can interact with the electron withdrawing oxygen of -OH group of TiO₂. This interaction is named the Lewis acid-base interaction, which is known to improve the polymer/filler interface. The improvisation of the polymer surface leads to the elimination of non-selective voids as it can be possible [16].

Apart from that, as per [14] The FTIR spectra of Psf/TiO₂/PEG were affected by the molecular weight of PEG, and these spectra showed distinctive absorption bands of =C-H vibration in aromatic rings at 1650 cm^{-1} as well as slight -C-H vibration in aliphatic at 2800 cm^{-1} . This is due to the fact that sample M6's peak grows stronger the longer the PEG chain is. Therefore, the quality of the polymer/filler interface can be enhanced by the correct chemical

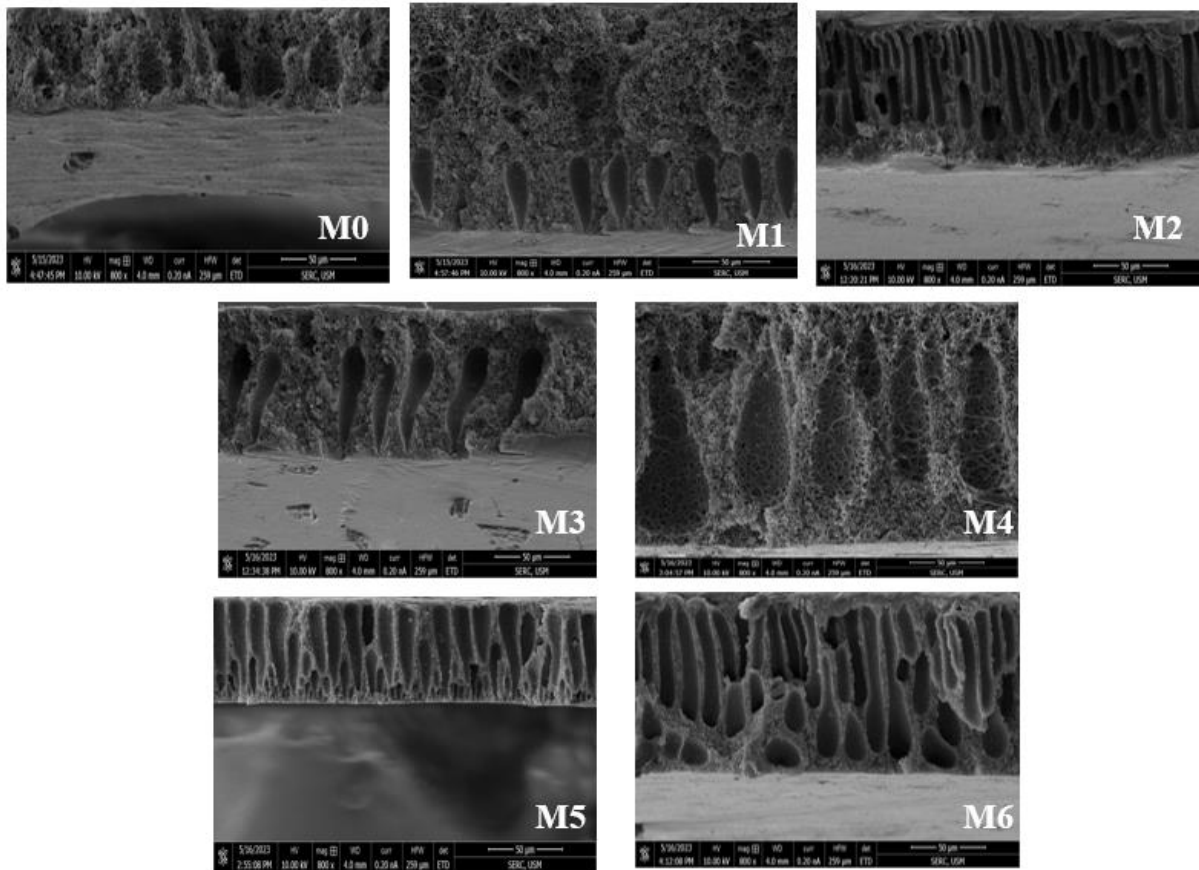
interactions inside membranes. In general, the TiO₂'s -OH group of electron-withdrawing oxygen and the positively charged double C=C groups of PEG may interact. The polymer/filler interface is improved by the Lewis acid-base interaction, which prevents non-selective voids to the extent that is practical [16]. Thus, the fact that M6 exhibited the strongest IR spectrum is due to the presence of long-chain functional groups in PEG.

3.2. Scanning Electron Microscopy (SEM)

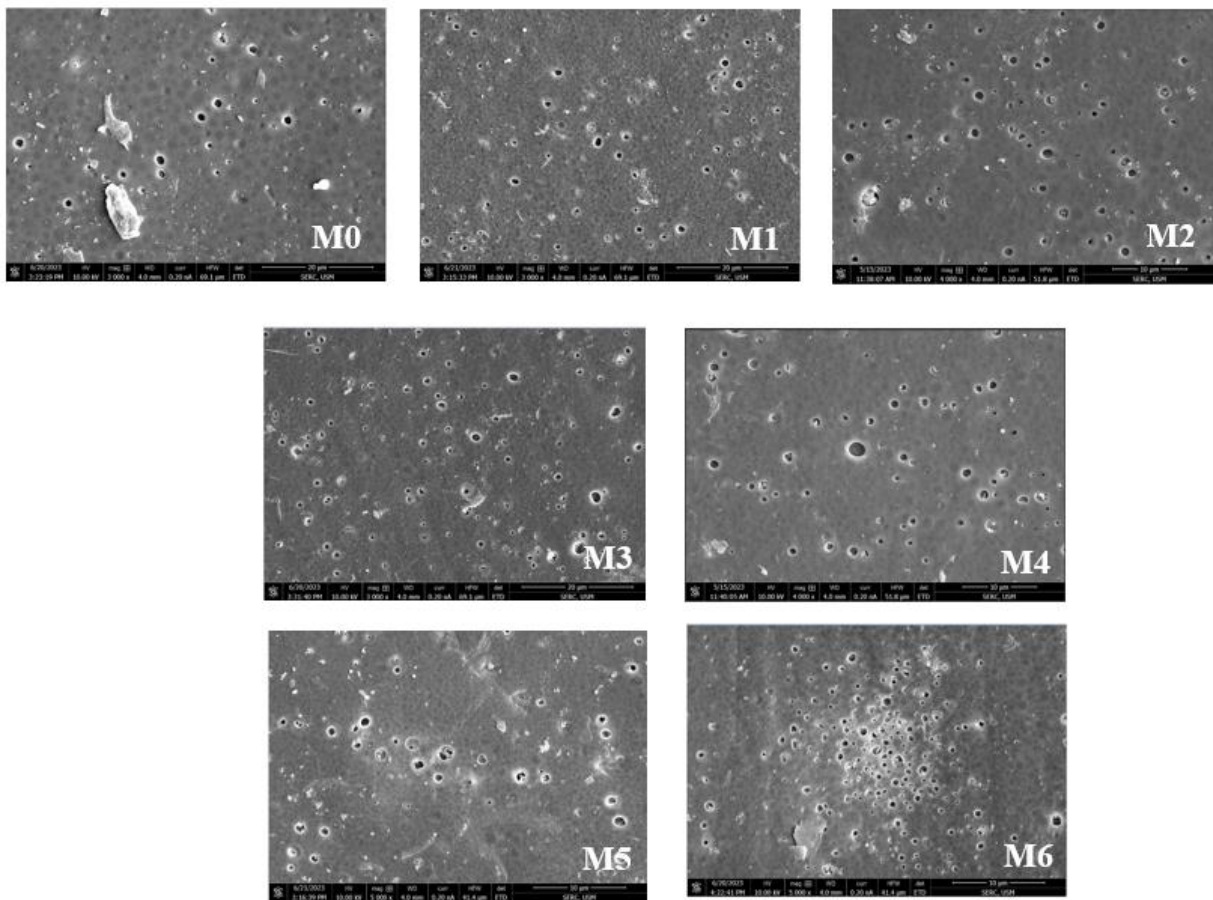
SEM analysis was done on all seven samples for both top surface and cross-section on the active site of the membranes. It is crystal clear that the inclusion of PEG and TiO₂ reflects on the morphology of the membrane in terms of structure and pore distribution. Pure PSF membrane M0 is the only membrane that lacks both PEG and TiO₂. Psf is super hydrophobic in nature, whereas PEG and TiO₂ are known to exhibit hydrophilic properties. Hence, these properties were tested by altering the surface of the polymer membrane. Pore size is directly impacted by the molecular weight of PEG. The formation of more porous membranes is correlated with greater molecular weights of PEG and bigger pore sizes. The surface morphology of each of the fabricated MMMs is presented in Figure 2 for both the top surface and cross-sectional area of the membrane.

The top surface morphology of membranes shows an increase in pore size with the molecular weight of PEG and inclusion of TiO₂. According to [18], this phenomenon is caused by the casting solution's increased hydrophilicity. An increase in the casting solution's hydrophilicity eventually leads to faster de-mixing between the solvent and non-solvent during membrane formation. However, there was fewer pore distributions on the surface of M0 compared to other membrane samples. This fewer pore distributions is owing to the absence of pore formers in the raw PSF MMMs. Although the pores were smaller, the surface pore distributions of Psf MMMs were consistent. This consistent morphology demonstrates that the membrane drying technique was carried out correctly [19].

Moving on with the cross-sectional morphology as molecular weight of PEG increases, as the molecular weight of PEG increases, the morphology of the cross-sectional structure view appears to have a more uniform pattern. This phenomenon can be attributed to the strong adhesion developed between Psf and PEG in the membrane. The alteration in the consistency of a uniform-shaped Psf owes to the interaction between the carbon-carbon double bond C=C and the open oxygen in the Psf chain. Based on the Figure 2, it can be seen that the morphology on the upper layer of the cross-section area tends to be denser with the increase in concentration of PEG. The increase in PEG molecular weight contributes to a more reliable and viscous solution. [20] states that it takes more time for larger concentrations of PEGs to reach the surface, permitting accumulation of polymers on the top surface, enabling a dense layer. Moreover, the lower weight of PEG is very soluble and has high chances of being washed off during the coagulation bath. The increase in the porous finger-like structure on the membranes is accredited by the increase in



(a)



(b)

Figure 2. The SEM micrographs of PSF MMMs (a) top surface at $2000\times$ magnification and (b) cross section at $800\times$ magnification

molecular weight of PEG. This statement is supported by a previous study of [21], which found that inclusion of higher molecular weights of PEG results in the formation of macrovoids of increased number and size, thus contributing to the development of many finger-like pores on the membrane.

The broad finger-like pattern became more prominent as PEG's molecular weight increased from 600 to 6000. For example, the expanded width size ranges from 3.5 m to 9.5 m for membranes M0 to M6, respectively, according to [22]. Apart from the benefits that PEG has to offer, TiO₂ also plays a crucial role in the cross-sectional morphology of membranes. The combination of PEG along with TiO₂ showcases a more uniform pattern. The -OH group of TiO₂ interacts with the -CH₂ group of PEG, allowing the polymer to efficiently interact with the filler while preventing non-selective interface gaps from developing. Furthermore, due to NP integration, the M2 membrane had a shorter finger-like shape with significant macrovoid dimensions and lengths. The inclusion of TiO₂ and PEG procastinated the solvent exchange rate with the coagulation bath, resulting in the development of a spongy structure together in M3 and M4. The speedy exclusion of solvent molecules in the coagulation bath is the aftermath of macrovoid formation. Membranes M5 and M6 were discovered to be the most porous membranes, which was in good agreement with [23]. This statement can be buttressed with the finger-like structure, bigger pore size, and irregular, large void that cannot be witnessed in M0 and M1. Hence, it is obvious that the fusion of both additives and nanoparticles showed up in increased pore distribution.

3.3. Contact Angle (CA) Evaluation

A contact angle (CA) evaluation was conducted to measure the wettability of a membrane's surface, or, in other words, to indicate the hydrophilicity or hydrophobicity of a membrane. The hydrophilicity of a membrane affects many aspects, such as fouling tendency, permeate flux, and rejection ability [24]. These factors are critical because they reflect the membrane's overall performance. The angle between a water droplet on the membrane surface was assessed to observe the effect of TiO₂ and PEG on the PSf membrane. The images captured in the Angle Meter PRO Plus software, along with the contact angle of M0 until M6, are displayed in Figure 3.

Neat Psf membrane, M0 obtained the highest contact angle of 73°, while the lowest CA attained was 48° by M6 of Psf/PEG 6000/TiO₂. The lower the contact angle is, the more hydrophilic the membrane will be. The introduction of hydrophilic additives such as TiO₂ and PEG, which contain hydroxylic groups in the membrane matrix, resulted in a gradual reduction for water contact angle values in the following sequence M0>M1>M2>M3>M4>M5>M6.

[25] statements were proven when the CA of decreased from 73° to 70° during the addition of TiO₂ in M1. The same occurrence then happened as molecular weight of PEG increased from 600 up to 6000 causing the CA to drop

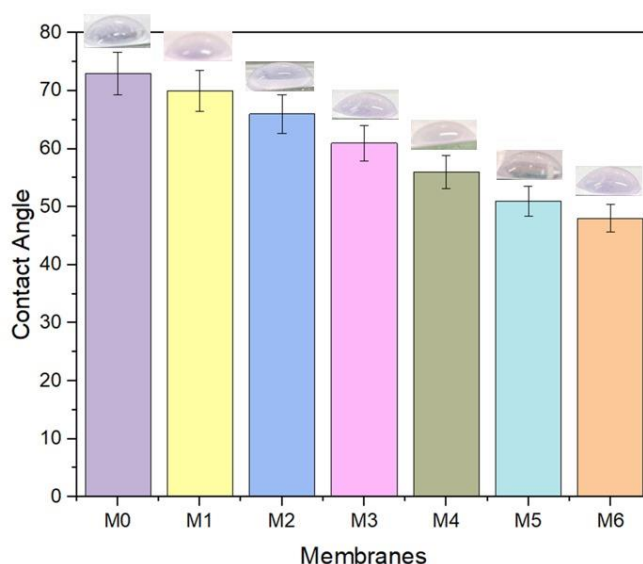


Figure 3. Contact angle of membranes M0 until M6

from 66° to 48°. This also concludes that the addition of PEG and TiO₂ increases the wettability of the membrane which reduces membrane's fouling tendency [26]. Moreover, PEG creates hydration layer with the aid of hydrogen bonds that are extremely simple to generate and break during the immersed phase inversion process. These hydrogen bonds assists in the formation of pores on membrane enhancing membrane hydrophilicity and permeability.

3.4. Membrane Porosity and Mean Pore Size

The mean size of holes on the membrane surface is described as the mean pore size, or, in other words, it can be said as the particle size that can be rejected by the membrane. Due to the amorphous nature of the polymeric thin-film membranes, it is unable to fabricate an ideal isoporous membrane. Therefore, the pores are distributed over a range of pore sizes [27], [28]. Both the porosity and mean pore size values of membranes M0–MM6 are tabulated in Table 2.

Based on the results, it can be seen that M0, pure Psf membrane exhibited the lowest porosity due to certain reasons such as the absence of NPs and additives in membrane when compared with other MMMs. This result is supported by [29] stating that the porosity of Psf was the lowest compared to other blended membrane which was about 40%. As can be observed, M6 Psf/TiO₂/PEG 6000

Table 2. The overall membrane porosity and mean pore size of fabricated MMMs

Membrane	Porosity (%)	Mean pore size (nm)
M0	28.72	22.91
M1	29.27	23.94
M2	45.12	26.77
M3	59.08	30.85
M4	62.26	32.68
M5	68.06	39.16
M6	71.63	43.66

membrane attained the highest porosity of 71.63%. This was attributed to the rapid demixing of the dope solution and led to speedy intrusion of distilled water into the membrane matrix.

Apart from that, M1 Psf/TiO₂ membrane has a lower porosity of 29.27% compared to M2 Psf/ TiO₂/PEG 600 which achieved a porosity of 45.12%. This may be caused by the TiO₂ aggregation resulting in blocked membrane pores [30]. Adding 1.5% PEG to the Psf/TiO₂ membrane increased surface porosity proving that incorporation of PEG additive enhanced surface porosity with a difference of 15.85%. The overall porosity of the fabricated MMMs incorporated with NPs is to be sequenced in an order of M6>M5>M4>M3>M2>M1. The creation of macrovoids and channels during the phase inversion process under the fast movement of water molecules was associated with the greater porosity of membranes. Hence, this incident contributes to the increase in membrane matrix's permeability and porosity.

3.5. Membrane Performance on UF Psf MMM

3.5.1. PWF and Cu Flux Correlation

Figure 4 illustrates the relationship between pure water flux and copper flux of membranes M0 until M6. From the Figure 4, it can be obviously concluded that PWF and Cu flux are directly proportional to each other. It can be denoted that as PWF increases, Cu flux also tends to increase. This phenomenon proves that the addition of PEG and TiO₂ embedded in Psf MMMs have created an effect on the dependence between PWF and Cu flux. Alongside, PEG incorporation also impacts the structure as well as membrane performance. The amount of PEG used and its molecular weight have a major impact on performance of polymer membranes. This statement is supported by [31] when he investigated the influence of PEG 400 Da, PEG 600 Da, PEG 1000 Da, PEG 1500 Da, PEG 4000 Da, and PEG 6000 Da molecular weights on Psf formation and determined that PEG can be regarded a pore former [28].

The reason why quantity and molecular weight of PEG should be taken into consideration is to enhance the mechanical capacity of the membrane [25]. Hence, the increase in molecular weight of PEG increases porosity, area of pores, hydraulic permeability, and pure water flux. The addition of TiO₂ and PEG directly impacts the porosity and hydrophilicity of the membrane due to its properties of being a nanoparticle that has exceptional separation

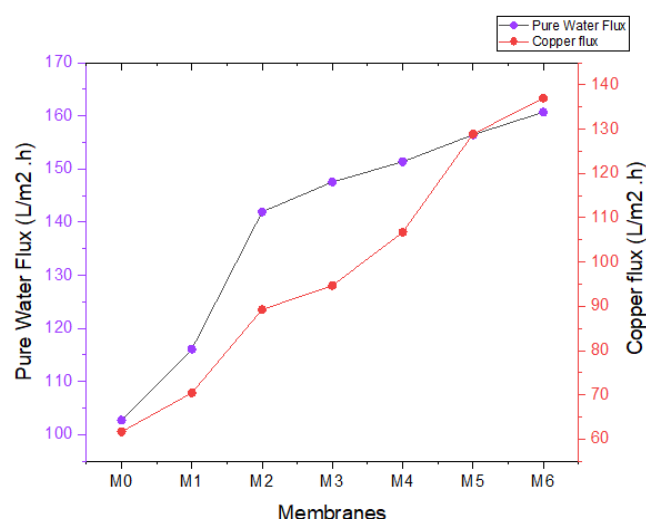


Figure 4. Correlation of pure water flux and copper flux

capabilities as well as acting as a pore former, respectively. Hence, when pore formers are introduced, it not only produces more pores to allow ease separation; instead, it also makes the membrane hydrophilic and reduces fouling. Hence, the combination of both PEG and TiO₂ has resulted in a membrane with properties that impact the pure water flux. As pure water flux is increased, it automatically reflects on the Cu flux due to their linear relationship.

Thus, PWF has gradually increased with M0, pure Psf membrane up to M6 PEG 6000 membrane. The trend increases along with the molecular weight of PEG from PEG 600, PEG 1000, PEG 1500, PEG 4000 and PEG 6000 in membranes M2, M3, M4, M5 and M6 respectively. To summarise, the addition of PEG 600 in M2 transpired in an appreciable shootup in pure water flux from M1 to M2, resulting in a bigger dissipation of pores. Following that, the fluxes gradually increased from M2 to M6.

3.5.2. Copper Rejection (R_{Cu})

All membranes were put under filtration test with 0.5 g/L copper solution, respectively. The copper rejection (R_{Cu}) of all fabricated MMMs in filtering the Cu solution is tabulated in Table 3. The neat PSF membrane recorded the lowest copper rejection rate at 25.8%, while all modified membranes with the inclusion of TiO₂ and PEG gradually showed an increase in the rejection percentage. The incorporation of NPs and polymer additives within the membrane matrix has an impact on the rejection

Table 3. The initial PWF, Cu permeate flux and final PWF and Cu rejection rate

Membrane	Initial PWF, J _{WF1} (L/m ² ·h)	Cu permeate flux, J _{Cu} (L/m ² ·h)	Final PWF, J _{WF2} (L/m ² ·h)	Retained of Cu on membrane (%)
M0	114.73	61.64	102.74	25.8
M1	126.51	70.41	116.10	50.5
M2	151.51	89.25	141.92	62.2
M3	156.78	94.66	147.53	67.9
M4	159.66	106.71	151.37	70.5
M5	161.99	128.90	156.44	77.2
M6	164.73	136.99	160.68	80.3

performance that is expected due to the constant operating pressure. This can be seen in the percentage difference from M0 to M1 and M2. At 80.3%, M6 achieved the highest rejection of copper.

A hydroxyl layer is usually formed by high surface hydrophilicity during filtration, which repels the Cu molecules from penetrating through the membrane. Thus, improving Cu retained on the surface of the membrane. For membrane M6, the rejection capability was nearly about 81%, which explains the exchange between selectivity and permeation has been increased, while the permeate flux was rarely influenced. However, based on the previous study by [27], the maximum copper rejection was 96% with PEG 10000 and study by [29] rejected 92.9% with PEG10000. The rejection rate is lower due to the usage of PEG with a smaller molecular weight. This is due to the unavailability of raw materials in the laboratory, and the highest molecular weight PEG available was PEG 6000.

3.6. Membrane Fouling Analysis

Among all of the fabricated membranes, the M6 of Psf/TiO₂/PEG 6000 exhibited the highest flux recovery ratio (FRR) because of the presence of hydrophilic layer support on the membrane matrix. The pure Psf membrane, M0 membrane, had the lowest FRR value in both concentrations, which revealed high exposure to membrane fouling. After dead-end cell filtration was complete, the membrane was exposed to 15 minutes of washing below running distilled water so as to get rid of the bonded foulant on the surface of the membrane. Then, MMMs were carried out as usual to measure the initial JWF, followed by J_{Cu} and JWF₂. The relative flux reduction (RFR) was quantitatively calculated, and therefore the hydraulic clean-up properties of the membrane may well be assessed by the flux recovery ratio (FRR), as shown in Figure 5. To achieve the best efficiency, the membranes illuminated outstanding antifouling properties with low RFR and high FRR.

The ordinary method to examine membrane fouling mitigation is through FRR [30]. This method may demonstrate irreversible fouling with the presence of adsorption of foulant on surface of membrane. The higher value of FRR indicated a robust membrane resistance against fouling and low value of RFR indicated the lower likelihood of membrane fouling [28], [31]. The lowest RFR fell into M4, M5 and M6 which indicated lower chance of fouling. In order words, these three membranes had better antifouling ability compared to others. After membrane washing, the membrane permeability can be recovered through evaluating the cleaning efficiency by FRR value. M6 obtained the highest FRR value about 97.55% which implied high cleaning efficiency. Basically, a high number of research and studies have been targeted on the modification of membrane so as to achieve a feasible structure of antifouling property of membranes. Pure Psf membrane, M0 seems to experience serious fouling activity because of the hydrophobic properties of Cu that created it susceptible to Cu fouling. Each of the MMMs exhibited mild fouling with higher reversible fouling. As shown in Figure 5, M6 membrane displayed the highest percentage of FRR and

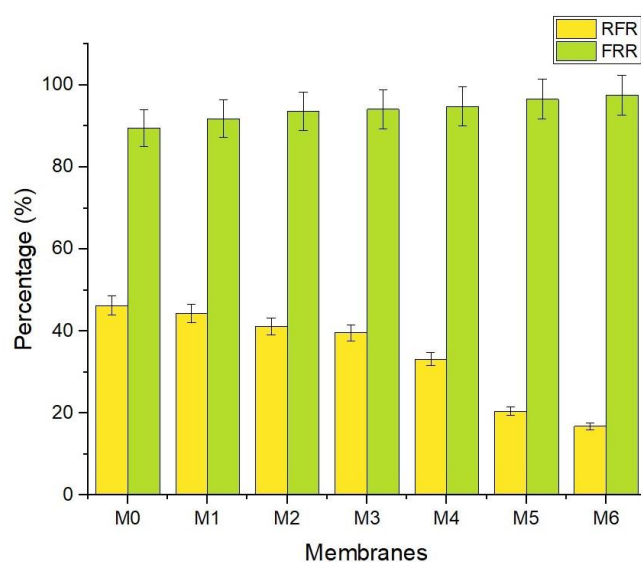


Figure 5. The antifouling properties of fabricated membranes.

lowest percentage of RFR in removal of Cu which confirmed the optimistic efficaciousness of the stated NPs and polymer additives within the improvement of fouling resistance characteristics of MMMs. This would reduce the cost in maintenance as well as sustainable filtration materials. Flux parameter is not associated with Cu solution because the pore blockage is observed on the membrane. In normal cases, we test the fouling analysis using water, hence when JWF₂ passes through well after the J_{Cu} test; this indicates that there are no deposition of impurities or foreign particles on the pores of the membrane.

4. CONCLUSION

In conclusion, all three objectives that mainly emphasized on the separation of copper from fabricated Psf MMMs were successfully achieved and proven in comparison to the commercial chemical method. The fabrication process via phase inversion method was a success with the inclusion of Psf, titanium dioxide (TiO₂) and polyethylene glycol (PEG). After fabrication, both chemical and physical analyses were conducted on the membranes by which both the analyses met the expected outcome. Fourier transform infrared (FTIR) spectrum was favourable whereby the absorption range of functional groups for Psf, TiO₂ and PEG was found overall. Moving on, with the morphological analysis for the fabricated Psf MMMs was shown the distribution of pores as well as the surface roughness of the membrane. M6 exhibited the highest number of pores on the membranes when compared to other Psf MMMs. Thus, membrane M6 attained the most hydrophilicity due to presence of PEG 6000. Both pure water flux (PWF) and copper flux (J_{Cu}) recorded a consistent growth pattern for all membranes.

The main findings from this research; out of all the fabricated MMMs, M6 Psf/PEG 6000/TiO₂ showed sensible permeation performance with higher copper rejection (R_{Cu}) about 80.3% against pristine Psf M0 which attained about 25.8% rejection due to its small pore size, high hydrophobicity as well as low porosity. This can be accredited to the molecular weight of PEG because the

higher the molecular weight of PEG, the greater number of pores formed on the membrane, thus it helps the permeability of small solutes in the membrane. In addition, reversible and irreversible fouling of Cu was also greatly improved, indicating that M6 has excellent antifouling capabilities. During the phase inversion process, the NPs employed in this research create a better interaction between the water flow and the hydrophilic NPs functional groups such as hydroxyl, carboxylic acid, and other functional groups. The synergistic impact of PEG and TiO₂ results in this improvement in R_{Cu} and antifouling by forming a protective coating that prevents foulants from bonding to the membrane surface. The findings of this study demonstrated that the Psf/TiO₂/PEG membrane is an optimal antifouling membrane, which may hold promise for novel applications in membrane technology.

ACKNOWLEDGMENTS

The author would like to thank to Universiti Malaysia Perlis (UniMAP) for providing financial support through Postgraduate Research Grant 9001-00747

REFERENCES

- [1] A. A. Kiss, J.-P. Lange, B. Schuur, D. W. F. Brilman, A. G. J. van der Ham, and S. R. A. Kersten, "Separation technology—Making a difference in biorefineries," *Biomass and Bioenergy*, vol. 95, pp. 296–309, 2016.
- [2] Y. He, D. M. Bagley, K. T. Leung, S. N. Liss, and B.-Q. Liao, "Recent advances in membrane technologies for biorefining and bioenergy production," *Biotechnology Advances*, vol. 30, no. 4, pp. 817–858, 2012.
- [3] R. Johnston, "Arsenic and the 2030 Agenda for Sustainable Development," in *Arsenic Research and Global Sustainability—Proceedings of the 6th International Congress on Arsenic in the Environment*, 2016, pp. 12–14.
- [4] A. Khan, T. A. Sherazi, Y. Khan, S. Li, S. A. R. Naqvi, and Z. Cui, "Fabrication and characterization of polysulfone/modified nanocarbon black composite antifouling ultrafiltration membranes," *Journal of Membrane Science*, vol. 554, pp. 71–82, 2018.
- [5] Y. Ibrahim, V. Naddeo, F. Banat, and S. W. Hasan, "Preparation of novel polyvinylidene fluoride (PVDF)-Tin(IV) oxide (SnO₂) ion exchange mixed matrix membranes for the removal of heavy metals from aqueous solutions," *Separation and Purification Technology*, vol. 250, p. 117250, 2020.
- [6] A. Esmaeili, S. Ghasemi, and J. Sohrabipour, "Biosorption of copper from wastewater by activated carbon preparation from alga *Sargassum* sp.," *Natural Product Research*, vol. 24, no. 4, pp. 341–348, 2010.
- [7] A. L. Ahmad, A. A. Abdulkarim, Z. M. H. Mohd Shafie, and B. S. Ooi, "Fouling evaluation of PES/ZnO mixed matrix hollow fiber membrane," *Desalination*, vol. 403, pp. 53–63, 2017.
- [8] N. Işıklan and O. Şanlı, "Separation characteristics of acetic acid–water mixtures by pervaporation using poly(vinyl alcohol) membranes modified with malic acid," *Chemical Engineering and Processing: Process Intensification*, vol. 44, no. 9, pp. 1019–1027, 2005.
- [9] S. K. Mishra, S. N. Tripathi, V. Choudhary, and B. D. Gupta, "Surface Plasmon Resonance-Based Fiber Optic Methane Gas Sensor Utilizing Graphene-Carbon Nanotubes-Poly(Methyl Methacrylate) Hybrid Nanocomposite," *Plasmonics*, vol. 10, no. 5, pp. 1147–1157, 2015.
- [10] A. A. Bunaciu, E. gabriela Udriştioiu, and H. Y. Aboul-Enein, "X-Ray Diffraction: Instrumentation and Applications," *Critical Reviews in Analytical Chemistry*, vol. 45, no. 4, pp. 289–299, 2015.
- [11] S. Zhang, Y. Tang, and B. Vlahovic, "A Review on Preparation and Applications of Silver-Containing Nanofibers," *Nanoscale Research Letters*, vol. 11, no. 1, p. 80, 2016.
- [12] S. Abdi, M. Nasiri, S. Yuan, J. Zhu, and B. Van der Bruggen, "Fabrication of PES-based super-hydrophilic ultrafiltration membranes by combining hydrous ferric oxide particles and UV irradiation," *Separation and Purification Technology*, vol. 259, p. 118132, 2021.
- [13] B. Mbuli, M. Mahlambi, C. J. Ngila, and R. Moutloali, "Polysulfone Ultrafiltration Membranes Modified with Carbon-Coated Alumina Supported NiTiO₂ Nanoparticles for Water Treatment: Synthesis, Characterization and Application," *Journal of Membrane Science and Research*, vol. 5, no. 3, pp. 222–232, 2019.
- [14] K. Kalantari, P. Moradihamedani, N. A. Ibrahim, A. H. Bin Abdullah, and A. B. M. Afifi, "Polysulfone mixed-matrix membrane incorporating talc clay particles for gas separation," *Polymer Bulletin*, vol. 75, no. 8, pp. 3723–3738, 2018.
- [15] K. Karimi, M. Tabatabaei, I. Sárvári Horváth, and R. Kumar, "Recent trends in acetone, butanol, and ethanol (ABE) production," *Biofuel Research Journal*, vol. 2, no. 4, pp. 301–308, 2015.
- [16] H. Sanaeepur, R. Ahmadi, A. Ebadi Amooghin, and D. Ghanbari, "A novel ternary mixed matrix membrane containing glycerol-modified poly(ether-block-amide) (Pebax 1657)/copper nanoparticles for CO₂ separation," *Journal of Membrane Science*, vol. 573, pp. 234–246, 2019.
- [17] S. Karimi, E. Firouzfar, and M. R. Khoshchehreh, "Assessment of gas separation properties and CO₂ plasticization of polysulfone/polyethylene glycol membranes," *Journal of Petroleum Science and Engineering*, vol. 173, pp. 13–19, 2019.
- [18] N. Koutahzadeh, M. R. Esfahani, and P. E. Arce, "Sequential Use of UV/H₂O₂—(PSF/TiO₂/MWCNT) Mixed Matrix Membranes for Dye Removal in Water Purification: Membrane Permeation, Fouling, Rejection, and Decolorization," *Environmental Engineering Science*, vol. 33, no. 6, pp. 430–440, 2016.
- [19] D. Nasirian, I. Salahshoori, M. Sadeghi, N. Rashidi, and M. Hassanzadeganroudsari, "Investigation of the gas permeability properties from polysulfone/polyethylene glycol composite membrane," *Polymer Bulletin*, vol. 77, no. 10, pp. 5529–5552, 2020.
- [20] M. H. Zahir, M. M. Rahman, K. Irshad, and M. M. Rahman, "Shape-Stabilized Phase Change Materials for Solar Energy Storage: MgO and Mg(OH)₂ Mixed

- with Polyethylene Glycol," *Nanomaterials*, vol. 9, no. 12, p. 1773, 2019.
- [21] A. Razmjou, J. Mansouri, and V. Chen, "The effects of mechanical and chemical modification of TiO₂ nanoparticles on the surface chemistry, structure and fouling performance of PES ultrafiltration membranes," *Journal of Membrane Science*, vol. 378, no. 1-2, pp. 73-84, 2011.
- [22] T. A. Agbaje, S. Al-Gharabli, M. O. Mavukkandy, J. Kujawa, and H. A. Arafat, "PVDF/magnetite blend membranes for enhanced flux and salt rejection in membrane distillation," *Desalination*, vol. 436, pp. 69-80, 2018.
- [23] A. Moslehyani, A. F. Ismail, T. Matsuura, M. A. Rahman, and P. S. Goh, "Recent Progresses of Ultrafiltration (UF) Membranes and Processes in Water Treatment," in *Membrane Separation Principles and Applications*, Elsevier, 2019, pp. 85-110.
- [24] M. S. Seyed Dorraji and V. Vatanpour, "Organic-inorganic composite membrane preparation and characterization for biorefining," in *Membrane Technologies for Biorefining*, Elsevier, 2016, pp. 85-102.
- [25] Y. Ma, F. Shi, J. Ma, M. Wu, J. Zhang, and C. Gao, "Effect of PEG additive on the morphology and performance of polysulfone ultrafiltration membranes," *Desalination*, vol. 272, no. 1-3, pp. 51-58, 2011.
- [26] G. P. Syed Ibrahim, A. M. Isloor, A. Al Ahmed, and B. Lakshmi, "Fabrication and Characterization of Polysulfone-Zeolite ZSM-5 Mixed Matrix Membrane for Heavy Metal Ion Removal Application," *Journal of Applied Membrane Science & Technology*, vol. 18, no. 1, 2017.
- [27] Y. Tang, Y. Lin, W. Ma, and X. Wang, "A review on microporous polyvinylidene fluoride membranes fabricated via thermally induced phase separation for MF/UF application," *Journal of Membrane Science*, vol. 639, p. 119759, 2021.
- [28] K. Pusphanathan *et al.*, "Efficiency of Fabricated Adsorptive Polysulfone Mixed Matrix Membrane for Acetic Acid Separation," *Membranes*, vol. 13, no. 6, p. 565, 2023.
- [29] T. van den Berg and M. Ulbricht, "Polymer Nanocomposite Ultrafiltration Membranes: The Influence of Polymeric Additive, Dispersion Quality and Particle Modification on the Integration of Zinc Oxide Nanoparticles into Polyvinylidene Difluoride Membranes," *Membranes*, vol. 10, no. 9, p. 197, 2020.
- [30] M. Soliman, Y. Al-Zeghayer, A. S. Al-Awadi, and S. Al-Mayman, "Economics of Acetic Acid Production by Partial Oxidation of Ethane," *APCBEE Procedia*, vol. 3, pp. 200-208, 2012.
- [31] S. Sakarkar, S. Muthukumaran, and V. Jegatheesan, "Tailoring the Effects of Titanium Dioxide (TiO₂) and Polyvinyl Alcohol (PVA) in the Separation and Antifouling Performance of Thin-Film Composite Polyvinylidene Fluoride (PVDF) Membrane," *Membranes*, vol. 11, no. 4, p. 241, 2021.